View metadata, citation and similar papers at core.ac.uk

brought to you by CORE

provided by Repository@USM

GROWTH OF ZnO NANORODS USING HYDROTHERMAL AND MODIFIED CHEMICAL BATH DEPOSITION FOR DEVICE APPLICATIONS

SABAH M. MOHAMMAD

UNIVERSITI SAINS MALAYSIA

2017

GROWTH OF ZnO NANORODS USING HYDROTHERMAL AND MODIFIED CHEMICAL BATH DEPOSITION FOR DEVICE APPLICATIONS

by

SABAH M. MOHAMMAD

Thesis submitted in fulfillment of the requirements

for the degree of

Doctor of Philosophy

March 2017

ACKNOWLEDGEMENT

In the name of Allah, Most Gracious, Most Merciful

First and foremost, I thank the Almighty Allah for granting me health, patience, and inspiration to complete this research.

I am deeply thankful to my main supervisor, Prof. Dr. Zainuriah Hassan for her excellent scholar guidance, intellectual support, and continuous support for my Ph.D study and related research. Thanks again for having your door open every time I needed help.

I would also like to thank my co-supervisor Dr. Naser Mahmoud Ahmed for his insight comments and encouragement, and support throughout this study.

I am also very grateful to Universiti Sains Malaysia for providing financial support for my research and for giving me the chance to be a graduate assistant. I also express appreciation to the staff of the Nano-Optoelectronics Research and Technology Laboratory (NOR Lab) for their technical assistance during my laboratory work.

Finally, I would like to thank all my friends and colleagues for their support.

Sabah M. Mohammad
Penang, Malaysia. 2017

TABLE OF CONTENTS

ACKNOWLEDGEMENT ..... **ii**

TABLE OF CONTENTS ..... **iii**

LIST OF TABLES ..... **viii**

LIST OF FIGURES ..... **ix**

LIST OF ABBREVIATIONS ..... **xiii**

LIST OF SYMBOLS ..... **xv**

ABSTRAK ..... **xvi**

ABSTRACT ..... **xviii**

CHAPTER 1: INTRODUCTION **1**

1.1 Problem Statement 2

1.2 Thesis Objectives 5

1.3 Thesis Originality 5

1.4 Thesis Overview 6

CHAPTER 2: LITERATURE REVIEW AND THEORETICAL BACKROUND **8**

2.1 Introduction 8

2.2 General Properties of ZnO 8

2.2.1 Crystal Structure Properties of ZnO 9

2.2.2 Optical Properties of ZnO 10

2.3 Growth Methods of ZnO NRs 12

2.3.1 Growth Mechanism of ZnO NRs by CBD Method 13

2.3.2 Hydrothermal Growth of ZnO NRs on Highly Flexible Nylon 15

2.3.3 Direct Heat Substrate-Modified Chemical Bath Deposition (DHS-MCBD) Technique for Growth of Ultralong ZnO NRs 15

2.4 Metal-Semiconductor-Metal (MSM) Photodetector 18

2.5 Operational Parameters of Photodetectors 20

2.5.1 Current Gain 20

2.5.2 Responsivity 20

2.5.3 The Photoconduction Mechanism in ZnO NRs 21

2.6 Overview of ZnO Nanostructures for Gas Sensing 23

2.6.1 H_2 Gas Sensing Mechanism of ZnO NRs 23

2.7 Literature Review of Flexible Electronic Devices 25

2.7.1 Flexible UV Detectors Based on ZnO NRs 25

2.7.2 Flexible Gas Sensor Based on ZnO NRs 26

2.8 Light Emitting Diodes (LEDs) 28

2.8.1 Forward and Reverse Bias 29

2.8.2 Junction Breakdown 32

2.8.3 Electron and Hole Recombination in Semiconductors 32

2.8.4 Radiative Recombination Mechanisms 32

2.8.5 Literature Review of ZnO-Based LED 35

2.8.6 Homojunction and Heterojunction Structure of LED 37

CHAPRER 3: METHODOLOGY AND INSTRUMENTS 40

3.1 Introduction 40

3.2 Substrate Cleaning 40

3.3 Radio Frequency/Direct Current (RF/DC) Sputtering System 42

3.4 Thermal Treatment Processes 43

3.5 Thermal Analysis of Thermo-Nylon Substrate 44

3.6 Hydrothermal Synthesis of ZnO NRs 45

3.6.1 Hydrothermal Synthesis of ZnO NRs and Fabrication of MSM UV-PDs 45

3.6.2 Hydrothermal Synthesis of ZnO NRs and Fabrication of a MSM H_2 Gas Sensing Device 47

3.7 Synthesis of Ultra-Length ZnO NRs by DHS-MCBD Technique 49

3.7.1 Growth of Ultralong ZnO NRs on ZnO Seeded Silicon by DHS-MCBD Technique 54

3.7.2 Growth of Ultralong ZnO NRs Directly on Seedless p-GaN/sapphire by DHS-MCBD Technique 55

3.7.3 Fabrication of Nano-Size Junction LED 56

3.8 Structural, Morphological and Optical Characterizations 57

3.8.1 X-Ray Diffraction (XRD) 58

3.8.2 Field Emission Scanning Electron Microscopy (FESEM) and Energy Dispersive X-ray (EDX) Spectroscopy 59

3.8.3 Transmission Electron Microscopy (TEM) 60

3.8.4 Atomic Force Microscopy (AFM) 61

3.8.5 Photoluminescence (PL) Measurements 62

3.8.6 Raman Spectroscopy 63

3.8.7 Optical Absorption 63

3.9 Shadow Grid Mask 65

3.10 Device Characterization Techniques 66

3.10.1 Measurements of Ultraviolet (UV) Photodetector 66

3.10.2 Gas Testing System 67

3.10.3 Electroluminescence (EL) Measurements of LED 68

CHAPTER 4: RESULTS AND DISCUSSION: HIGHLY FLEXIBLE MSM UV PHOTODETECTOR DEVICES 70

4.1 Introduction 70

4.2 Thermal Properties of Substrate 70

4.3 Effect of Different Seed-Heat-Treatment Duration 72

4.4 Effects of Seed Heat Treatment Duration on Growth of ZnO NRs 75

4.5 TEM Images of ZnO NRs 77

4.6 Structural Characterization by X-ray Diffraction 79

4.7 Optical Properties of the Grown ZnO NRs Array 81

4.8 UV Detection Properties 82

4.9 Summary 85

CHAPTER 5: RESULTS AND DISCUSSION: HIGHLY FLEXIBLE HYDROGEN GAS SENSOR DEVICE 86

5.1 Introduction 86

5.2 Structural Characterization by X-ray Diffraction 86

5.3 Optical Properties of the Grown ZnO NRs 88

5.4 Current–Voltage (I-V) Characteristics of the Device (Pt/ZnO NRs/Pt) 90

5.5 Hydrogen Gas Sensing Property 91

5.6 Characterization of the Grown ZnO NRs 96

5.7 Summary 101

CHAPTER 6: RESULTS AND DISCUSSION: DHS-MCBD SYSTEM FOR THE GROWTH OF ULTRALONG ZnO NRs ON SEEDED SILICON AND SEEDLEES p-GaN SUBSTRATES AND FABRICATION OF A LED 102

6.1 Introduction 102

6.2 DHS-MCBD System for The Growth of Ultralong ZnO NRs on Seeded Silicon 102

6.2.1 Characterization of the Ultralong ZnO NRs 102

6.2.2 Energy-Dispersive X-ray Spectroscopy 105

6.2.3 Structural Characterization by X-ray Diffraction 105

6.2.4 Raman Spectroscopy 107

6.2.5 Photoluminescence (PL) Measurement 108

6.3 DHS-MCBD System for the Growth of Ultralong ZnO NRs on Seedless P-GaN and Fabrication of a Nano-Size Junction LED 110

6.3.1 Characterization of the Ultralong ZnO NRs 111

6.3.2 Structural Characterization by X-ray Diffraction 112

6.3.3 Raman Spectroscopy 113

6.3.4 Photoluminescence (PL) Measurements 114

6.3.5 Current-Voltage (I-V) Characteristics 116

6.3.6 Electroluminescence Characteristics 117

6.4 Summary 123

CHAPTER 7: CONCLUSION AND FUTURE STUDIES 124

7.1 Conclusions 124

7.2 Future Studies 126

REFERENCES 127

APPENDICES 146

LIST OF PUPLICATIONS

LIST OF TABLES

Page

Table 2.1: The diameter, length and aspect ratio of ZnO NRs grown using different fabrication methods and reported by several groups. 18

Table 2.2: Summary of flexible UV detector devices based on ZnO NRs with their different structure used, type flexible substrates, wavelength of light detection, response, decay times, responsivity, and current gain. 26

Table 2.3: EL spectra of LED fabricated using different fabrication methods. 39

Table 4.1: Structural parameters determined from (002) reflection, (FWHM full width at half maximum) and the determined optical band gap values for samples..... 80

Table 4.2: Dark current, photocurrent, responsivity and average aspect ratio with different time of heat treatment of ZnO seeded layer/nylon substrate..... 83

Table 5.1: Effect of temperature on the sensitivity, rise time, and recovery time of the fabricated device. 92

Table 5.2: Sensing properties of ZnO gas sensor obtained from previous and present work. 95

LIST OF FIGURES

Page

Figure 2.1: Crystal structure model of hexagonal wurtzite ZnO (a) hexagonal wurtzite crystal structure of ZnO [31], (b) polar faces, perpendicular to the 0001 direction, and non-polar faces, parallel to the 0001 direction [32]. 9

Figure 2.2: Schematic energy level diagram of various defect level emissions in ZnO [41, 42]. 12

Figure 2.3: A structure of a conventional MSM-PD: (a) the top of the surface and (b) cross-sectional views. 19

Figure 2.4: A schematic of UV-detection mechanism of ZnO NR with surrounding air: (a) the rod of ZnO in the dark condition and (b) the photogenerated electron-hole pairs during UV illumination. (c) energy band diagram during UV illumination [76]. 22

Figure 2.5: Schematic representations of energy band diagrams of a p-n junction under various biasing conditions. (a) Thermal equilibrium condition, (b) Forward bias condition, and (c) Reverse bias condition [108]. 30

Figure 2.6: Three types of semiconductor heterojunctions [116]. 31

Figure 2.7: The intrinsic radiative recombination in a semiconductor (direct band to band). 34

Figure 2.8: The extrinsic radiative recombination: (a) Donor state-valence band, (b) Conductive band-acceptor state, (c) Donor-acceptor recombination, and (d) Bound exciton annihilation. 35

Figure 3.1: Flowchart of the preparation processes for ZnO NRs, and fabrication of MSM PDs, H_2 gas sensor and nano-size junction LED devices. 41

Figure 3.2: Schematic of the fabrication procedure of MSM UV-PDs. 47

Figure 3.3: Schematic of the fabrication procedure of the hydrogen gas sensor. 49

Figure 3.4: Real optical photo of the direct heat substrate - modified chemical bath deposition (DHS-MCBD) apparatus in accordance with the present work. 53

Figure 3.5: Schematic figure of the direct heat substrate - modified chemical bath deposition (DHS-MCBD) apparatus in accordance with the present work. 54

Figure 3.6: A schematic diagram of n-ZnO NRs /p-GaN heterostructure LED in accordance with the procedure described in section 3.7.3. 57

Figure 3.7: Bragg diffraction in a crystal. The angles at which diffraction occurs are a function of the distance between planes and the X-ray wavelength [146]. 58

Figure 3.8: The real top-view microscopic image of ZnO NRs MSM photodetector device. 65

Figure 3.9: Schematic of experimental setup for photodetection measurements of the spectral response of the devices. 66

Figure 3.10: Gas sensor test system configuration. 68

Figure 4.1: DSC spectrum of the flexible nylon substrate. 71

Figure 4.2: TGA spectra of the flexible nylon substrate. 72

Figure 4.3: Surface morphology of ZnO seeds, (a) at room temperature and heat treated at 180 °C for (b) 0.5 h; (c) 3 h; (d) 6 h. 73

Figure 4.4: 3D-topography obtained by AFM of ZnO films over (3x3) μm^2 scan area (a) at room temperature and heat treated at 180 °C for (b) 0.5 h; (c) 3 h; (d) 6 h. 74

Figure 4.5: FESEM images of ZnO NRs grown onto ZnO seeds/nylon-substrate, (a) at room temperature and heat treated at 180 °C for (b) 0.5 h; (c) 3 h; (d) 6 h. 76

Figure 4.6: TEM images of ZnO NRs grown onto ZnO seeds/nylon substrates, (a) at room temperature and heat treated at 180 °C for (b) 0.5 h; (c) 3 h; (d) 6 h. 78

Figure 4.7: X-ray diffraction patterns of ZnO NRs formed onto ZnO seeds/nylon-substrate (a) at room temperature and heat treated at 180 °C for (b) 0.5 h; (c) 3 h; (d) 6 h. The insets show the peak (002) reflection. 79

Figure 4.8: Optical absorption spectra of the ZnO NRs on ZnO seeds /nylon substrate, (a) at room temperature and heat treated at 180 °C for (b) 0.5 h; (c) 3 h; (d) 6 h. The inset shows plot of $\alpha h\nu 2$ versus hν. 81

Figure 4.9: I-V characteristics of the fabricated MSM UV-photodectectors under UV illumination (Iph) (λ=365 nm) and in dark (Id). The inset shows the current gain-voltage curves. 83

Figure 5.1: X-ray diffraction pattern of ZnO NRs formed onto ZnO seed/nylon substrate. 87

Figure 5.2: Room-temperature PL spectrum of ZnO NRs formed onto ZnO seed/nylon substrate. The inset shows the zoom in on the PL in the range of wavelength =500 to 800 nm (DLE region). 89

Figure 5.3: I–V curves of the device (Pt/ZnO NRs/Pt) as prepared and annealed at 180 °C for 4 h. 91

Figure 5.4: Sensitivity and repeatability of ZnO NRs formed onto ZnO seed/nylon gas sensor at different sensor temperatures: (a) RT, (b) 75 °C, (c) 120 °C, and (d) 180 °C. 92

Figure 5.5: Real-time sensitivity of the ZnO nanorod array sensor upon exposure to H_2 with various concentrations (750, 1000, 1500, and 2000 ppm) at operating temperature of 75 °C. 94

Figure 5.6: FESEM images of ZnO NRs grown on ZnO seeds/nylon substrate at 90 °C for 3 h (high magnification and low magnification). The inset is the EDX spectrum. 98

Figure 5.7: Illustration of presumed paths for electrons through ZnO NRs and between two Pt electrodes. 98

Figure 5.8: TEM image of ZnO NRs grown onto ZnO seeds/nylon substrate. 99

Figure 5.9: The sensitivity versus time of the prepared device at an operating temperature of 100 °C, and under exposure to 500 ppm of H_2 for 45 min. 101

Figure 6.1: FESEM cross section images (different magnification) with 30° tilted views of ultralong ZnO NRs grown onto ZnO seeds/silicon-substrate. .. 104

Figure 6.2: EDX spectrum of ZnO NRs formed on ZnO seeds/silicon-substrate for the sample. 105

Figure 6.3: High-resolution X-ray diffraction pattern of ZnO NRs formed on ZnO seeds/silicon substrate. The inset shows the zoom in on the XRD pattern in the range of 2θ =31 to 38 degree. 107

Figure 6.4: Raman spectrum of ZnO NRs formed on ZnO seeds/silicon substrate. .. 109

Figure 6.5: Room-temperature photoluminescence spectrum of ZnO NRs formed on ZnO seeds/silicon substrate. 110

Figure 6.6: FESEM top-view and cross-sectional images (different magnification) with 30° tilted views of ZnO NRs grown on p-GaN/sapphire substrate, where the left inset shows EDX spectra of ZnO NRs grown on p-GaN/sapphire substrate. 112

Figure 6.7: X-ray diffraction pattern of ZnO NRs formed on p-GaN/sapphire substrate. 113

Figure 6.8: Room-temperature Raman spectra of p-GaN/sapphire substrate and n-ZnO NRs formed on p-GaN/sapphire substrate. 114

Figure 6.9: PL spectra of p-GaN/sapphire substrate and n-ZnO NRs formed on p-GaN/sapphire substrate. 116

Figure 6.10: I-V characteristics of n-ZnO NRs /p-GaN LED, where the bottom right inset shows the ohmic characteristic of Pd/ITO contact on p-GaN layer. 117

Figure 6.11: Room-temperature EL measurement spectra emission from back side of the n-ZnO NRs/p-GaN LED with different current injections at the reverse breakdown bias, where bottom right inset shows the zoom in on the EL spectra in the range of 450 to 550nm.Top right inset shows real optical photos of the LED in the ambient lighting at the current injection of 22 mA. 119

Figure 6.12: Room-temperature EL measurement spectra emission from front side of the n-ZnO NRs /p-GaN LED with different current injections at the reverse breakdown bias, where bottom right inset shows the zoom in on the EL spectra in the range of 450 to 650 nm. Top right inset shows real optical photos of the LED in the ambient lighting at the current injection of 22 mA. 120

Figure 6.13: Energy band diagram of n-ZnO NRs /p-GaN heterojunction at (a) zero and (b) reverse bias. 122

LIST OF ABBREVIATIONS

a. u.	Arbitrary unit
AFM	Atomic force microscope
E_g	Band gap energy
CBD	Chemical bath deposition
CVD	Chemical vapor deposition
CB	Conduction band
CFI	Continuous flow injection
I_{air}	Current in the presence of air atmosphere
I_H	Currents in the presence of hydrogen gas
I-V	Current-voltage
I_d	Dark current
DLE	Deep level emission
W	Depletion layer width
DSC	Differential scanning calorimetry
EL	Electroluminescence
EDX	Energy dispersive X-ray
E_F	Fermi level of semiconductor
FESEM	Field emission scanning electron microscopy
FWHM	Full width at half maximum
IR	Infrared radiation
LED	Light emitting diode
MOCVD	Metal–organic chemical vapor deposition
MSM	Metal–semiconductor–metal

MBE	Molecular beam epitaxy
NRs	Nanorods
1D	One-dimensional
I_{ph}	Photocurrent
PL	Photoluminescence
PVD	Physical vapor deposition
PC	Polycarbonate
PDMS	Polydimethylsiloxane
PES	Polyethersulfone
PEN	Polyethylene naphthalate
PET	Polyethylene terephthalate
PI	Polyimide
PLD	Pulsed laser deposition
RCA	Radio Corporation of America
RF	Radio frequency
R	Responsivity
RT	Room temperature
S	Sensitivity
TGA	Thermal gravimetric analysis
TEM	Transmission electron microscopy
UV	Ultraviolet
VB	Valence band
XRD	X-ray diffraction

LIST OF SYMBOLS

K_B	Boltzmann constant
$^{\circ}C$	Celsius temperature
θ	Diffraction angle
χ	Electron affinity
q	Electron charge
eV	Electron volt
e–h	Electron–hole
ν	Frequency
d_{hkl}	Interplant spacing of the crystal
n	Lattice constant
a, c	Lattice constants
hkl	Miller indices
h	Planck's constant
s	Second
ε_{zz}	Strain
t	Time
λ	Wavelength

PERTUMBUHAN NANOROD ZnO MENGGUNAKAN HIDROTERMA DAN PEMENDAPAN RENDAMAN KIMIA YANG DIUBAHSUAI UNTUK APLIKASI PERANTI

ABSTRAK

Zink oksida (ZnO) adalah semikonduktor jurang jalur lebar yang berpotensi dalam aplikasi peranti elektronik dan peranti optoelektronik berkecekapan tinggi. Kajian ini mengandungi dua objektif. Pertama, adalah untuk mensintesis nanorod (NRs) ZnO yang sejajar, menegak dan condong di atas substrat nilon melalui kaedah hidroterma, dan seterusnya memfabrikasikan pengesan foto ultra ungu (UV-PDs) yang berkos rendah dan sangat fleksibel dan peranti pengesan gas hidrogen (H_2). Pra-rawatan haba untuk benih/substrat ZnO pada suhu 180°C dengan pelbagai tempoh (0.5-6 jam) menunjukkan perubahan penting. Pemerhatian morfologi mendedahkan pembentukan sejajar nanorod berbentuk seperti heksagon apabila diameter, panjang (nisbah aspek), luas permukaan dan kepadatan meningkat dengan peningkatan masa rawatan haba. Analisis pembelauan sinar-X mengesahkan pembentukan fasa wurtzit ZnO bersama dengan orientasi pilihan (002) dan peningkatan penghabluran. Spektrum fotoluminesen mempamerkan puncak pemancaran pinggir jalur berhampiran ultraungu (UV) yang kuat dan tajam dan lebih tinggi berbanding daripada puncak lebar. Berdasarkan keputusan di atas, didapati bahawa suhu rawatan haba yang optimum dan jangka masa untuk menghasilkan benih ZnO seragam adalah 180°C selama 3 jam. Untuk pengesan UV logam-semikonduktor logam (MSM), filem yang optimum (3 jam) menunjukkan sambutan tertinggi dan nisbah arus 0.4774 A/W dan 9.15 masing-masing untuk cahaya UV pada 365 nm di bawah pincangan 5 V, ini disebabkan oleh nisbah permukaan-isipadu yang tinggi dan kualiti hablur yang

tinggi dengan kecacatan struktur yang kurang dalam NRs ZnO. Untuk sensor gas H_2, kepekaan dan masa tindak balas pengesan gas berasaskan ZnO untuk gas hidrogen pada suhu operasi yang berbeza dan dalam pelbagai kepekatan hidrogen telah disiasat. Di bawah pendedahan 500 ppm H_2 pada suhu yang berbeza daripada suhu bilik kepada 180 °C, kepekaan meningkat daripada 109% kepada 264%. Apabila gas H_2 yang didedahkan meningkat daripada 750 ppm hingga 2000 ppm pada suhu tetap 75 °C, kepekaan juga meningkat secara mendadak dari 246% hingga 578%. Selain itu, kedua-dua tindak balas dan masa pemulihan untuk peranti bagi kedua-dua ujian telah dipertingkatkan. Tujuan kedua kajian ini adalah untuk mensintesis NRs ZnO ultra panjang pada substrat berbiji dan tidak berbiji melalui teknik novel iaitu kaedah pemendapan rendaman kimia dengan haba langsung yang diubahsuai ke atas substrat (DHS-MCBD) dan seterusnya mengfabrikasikan peranti diod pemancar cahaya (LED) simpang saiz nano. Khususnya, sistem DHS-MCBD menyediakan satu kaedah yang mudah dan kos rendah untuk membentuk bahan filem berstruktur nano berskala tinggi pada substrat. Ia telah berjaya digunakan untuk mensintesis NRs ZnO menegak, ultra panjang, sejajar, dan berbentuk heksagon pada substrat silikon berbiji dan substrat p-GaN tidak berbiji. Ciri-ciri LED arus-voltan (I-V) mencadangkan bahawa kesan pecahan peranti ini disebabkan oleh kesan terowong di antara muka simpang hetero itu. Sifat luminesen peranti LED yang difabrikasikan telah disiasat dari kedua-dua bahagian LED pada suhu bilik dengan kaedah elektroluminesen (EL). Pemancaran spektrum EL dari bahagian belakang peranti itu terdiri daripada satu pancaran ultra ungu dan jalur lebar pancaran hijau, manakala pemancaran dari sebelah hadapan terdiri daripada pancaran ungu berhampiran dengan jalur lebar pancaran hijau. Pemancaran EL juga adalah cukup terang untuk dilihat dengan mata kasar di bawah pencahayaan bilik biasa.

GROWTH OF ZnO NANORODS USING HYDROTHERMAL AND MODIFIED CHEMICAL BATH DEPOSITION FOR DEVICE APPLICATIONS

ABSTRACT

Zinc oxide (ZnO) is a promising wide band gap semiconductor with applications in high efficiency electronic and optoelectronic devices. The present study follows two objectives. First, synthesis of vertical and inclined well-aligned ZnO nanorods (NRs) on a nylon substrate via the hydrothermal method, and subsequently fabricate the highly flexible low-cost ultraviolet photodiodes (UV-PDs) and hydrogen (H_2) gas sensor devices. Pre-heat treatment of ZnO seeds/substrate at 180°C with varying duration (0.5-6 h) shows important changes. Morphological observations revealed the formation of aligned hexagonal-like shaped nanorods when the diameter, length (aspect ratio), surface area and density increase with increasing heat treatment time. The X-ray diffraction analysis confirms the formation of wurtzite ZnO phase with a preferred orientation along (002) direction and enhanced crystallinity. Photoluminescence spectra exhibited a strong and sharp ultraviolet (UV) near band edge emission peak that was higher than that of the broad peak. According to the above results, it was found that the optimum heat-treatment temperature and duration to produce uniform ZnO seeds was 180°C for 3 h. For metal-semiconductor-metal (MSM) UV detectors, the optimized film (3 h) showed the highest responsivity and current gain of 0.4774 A/W and 9.15, respectively for UV light at 365 nm under a 5 V bias due to the high surface-to-volume ratio and high crystalline quality with less structural defects within ZnO NRs. For H_2 gas sensor,

the sensitivity and response time behaviors of the ZnO-based gas sensor to hydrogen gas at different operation temperatures and in various hydrogen concentrations were investigated. Under 500 ppm of H_2 exposure at different temperatures from room temperature to 180 °C, the sensitivity increased from 109% to 264%. When the exposed H_2 gas increased from 750 ppm to 2000 ppm at a fixed temperature of 75 °C, the sensitivity also sharply increased from 246% to 578%. Moreover, both the response and recovery time of the device during both tests were enhanced. The second aim of the study is to synthesize ultralong ZnO NRs on the seeded and seedless substrates via a novel technique, a direct heat substrate-modified chemical bath deposition (DHS-MCBD), and subsequently fabricate a nano-size junction light emitting diode (LED) device. In particular, DHS-MCBD system provides a simple and low-cost method for forming a high-scale nanostructured material film on a substrate. It has been successfully used to synthesize vertically, ultra-long, well-aligned, and hexagonal-shaped ZnO NRs on seeded silicon and seedless p-GaN substrates. Current–voltage (I–V) characteristics of the LED suggested that the breakdown effect of the device is caused by tunnelling effect at the interface of the heterojunction. The luminescence properties of the fabricated LED device were investigated from both sides of LED at room temperature by electroluminescence (EL). EL spectrum emission from back side of the device was composed of an ultraviolet emission and a broad band around green emission, while the emission from front side was composed of a near violet emission with a broad band green emission. EL emission was also bright enough to be seen with the naked eye under normal room illumination.

CHAPTER 1: INTRODUCTION

Zinc oxide (ZnO) semiconductor is of great interest because of its significant and unique properties, such as a wide direct energy gap (3.37 eV), thereby a high transparency in the visible light with a large exciton binding energy (≈60 meV), hence making it luminous efficiency at room temperature comparable with other competitive materials. In addition, it is considered as low cost material, nontoxic and suitable for operating in the ultraviolet (UV) wavelength regions [1, 2]. Among various oxide compounds, ZnO nanostructures present a large interest because of their important and unique properties for a huge range of nanotechnology applications such as UV detectors, chemical sensors, biosensors, pH sensors and UV light emitting devices (LEDs) [3].

Various synthesis methods have been recently developed for 1D ZnO nanomaterial growth, including hydrothermal or wet chemical methods [4], molecular beam epitaxy (MBE) [5], metal–organic chemical vapor deposition (MOCVD) [6, 7], pulsed laser deposition (PLD) [8], top-down approaches by etching [9], electrospinning [10, 11], and physical vapor deposition (PVD) [12, 13], and sputtering [14]. Although each synthesis technique offers unique advantages/disadvantages, the chemical bath deposition (CBD) or hydrothermal deposition is generally an inexpensive and facile method for the deposition of ZnO nanorods (ZnO NRs)-arrays over large areas. In 2001, Vayssieres et al. proposed an inexpensive process for fabricating highly oriented ZnO nanorods-arrays directly onto various type of substrates [15].

Shortly after Nakamura solved the p-type doping problem [16], the researchers have focused on the GaN material, leading to the wide commercialization

of GaN-based visible/blue/ultraviolet LEDs, lasers, and photodetectors. Currently, almost all commercial LEDs for solid-state lighting are manufactured by GaN material. Despite the potential of commercialization of the ZnO-based LEDs has been hampered by issues of simultaneously reducing intrinsic n-type doping semiconductor material as well as the fabrication of the stability and reliability of p-type ZnO still present a great challenge [17], ZnO is considered to be a potentially superior material for use in LEDs and laser diodes. Because of its much larger exciton binding energy (60 meV) compared to 21 meV for GaN (thermal energy at room temperature is about 25 meV), this means that one can expect out brighter and more robust excitonic-based ZnO emitters [18]. On the other hand, noble metals, such as GaN, SiC, etc, are always costly. Therefore, ZnO is a promising candidate for commercialization in a wide variety of applications [19]. Indeed, ZnO NRs-based UV-blue LEDs have been widely reported in the literature and a material that holds much promise for the future of solid-state lighting [20].

1.1 Problem Statement

Several essential problems addressed in this thesis, are summarized as follows:

Nowadays, flexible substrates have been widely used for fabrication of electronic portable devices because of their interesting properties such as thinness, flexibility, transparency, transportability, resistance to degradation or impact damage, light weight, rollable, and low cost. The flexible electrical devices such as photodetectors, gas sensors, and others offer a number of advantages compared with the rigid electrical devices. As a result, such devices are more potential to be applied in the future, especially with increasing demand for portable applications. However,

flexible electronic devices are rapidly developing due to the need of the modern technology for the electrical applications that are light weight, mechanically flexible, and reduced in size. Obviously, a substrate plays a key role and hardly to be a single factor in determining the extent of flexibility or rigidity for any processes of fabrication of electronic device. It is worth mentioning that the thickness of the base plays an important role in setting its flexibility, in which the flexibility increases when its thickness is reduced [21]. Therefore, it is crucial and beneficial to add a new flexible substrate with advanced specifications such as ultra-thin and high flexibility, to the field of fabrication of the flexible electrical devices. In spite of its importance, there has not been an extensive research on this issue.

Most synthesis methods for ultralong ZnO nanorods (NRs) arrays require high temperature, therefore such methods consume more energy and as a result, are expensive. Meanwhile, these methods are complex instruments. However, it is still difficult and challenging to fabricate ultralong ZnO nanorods arrays in order to obtain a high aspect ratio by the chemical bath deposition (CBD). This problematic issue might be due to two main reasons. First, it is because of decreasing in the concentration of a solution (source of ions) in the bath during growth with increase in duration of reaction. Second, it is because of supplying thermal energy indirectly usually in CBD method on a substrate in which the solution is heated. Another disadvantage of this method is that it is difficult to increase the temperature of a substrate because any increase in temperature of bath more than 100 $^{\circ}$C leads to boiling of the solution that may cause inhomogeneous growth and undesirable contamination on the substrate.

To reduce a negative property in heterojunction case and increase the carrier injection efficiency, manufacturing of a nano-sized junction has been suggested by fabricating an n-ZnO NRs on p-GaN substrate instead of n-ZnO layer. In order to synthesise ZnO NRs on a substrate by CBD technique (or other low temperature methods), many researchers have proposed the deposition of seeds/layer between ZnO and a substrate or the use of some catalysts because the seed layer plays a significant role in fabricating the rods of ZnO on a substrate.

Although the mismatch between both materials such as ZnO and GaN is small, the fabricating of ZnO on GaN without seed layer has still been a major challenge due to low growth temperature. Meanwhile, there are many disadvantages in using the ZnO seed layer between n-type and p-type materials such as increasing the density of interfacial defects [22, 23]. Hence, the absence of interface layer (such as ZnO seed layer) between ZnO and GaN whereby the rods of ZnO start to grow directly from the surface of GaN layer which leads to the fabrication of a nano-sized junction between ZnO and GaN. It shows that the properties of ZnO NRs are related to the nature of GaN substrate.

In addition, the nano-size junction between ZnO and GaN plays an important role in enhancing the luminescence efficiency property of LED device that increases carrier tunneling efficiency through the junction [24-26]. Furthermore, this phenomenon can also be useful for other device applications, such as sensor, photodetector, and transistor, and so on.

1.2 Thesis Objectives

The main objectives of this thesis can be summarized in the following points:

1. To study the characteristics of vertically well-aligned ZnO NRs arrays grown by the low-temperature hydrothermal technique on a novel nylon substrate
2. To determine the optimum heat treatment duration applied to ZnO seed layer deposited on the flexible nylon substrate.
3. To investigate UV detection and gas sensing properties of the highly flexible metal-semiconductor-metal (MSM) UV photodetector and H_2 gas sensor devices, respectively.
4. To study the characteristics of vertically well-aligned ultra-long ZnO NRs arrays synthesized via DHS-MCBD technique on the Si seeded and GaN seedless substrates, and to investigate electroluminescence (EL) of the nano-size junction LED device.

1.3 Thesis Originality

The originality of this research work can be based on the following aspects:

1. A hydrothermal method for the growth of ZnO NRs on a cheap, ultrathin (15 μm), and highly flexible nylon substrate is used.
2. The effects of the heat treatment duration applied to the ZnO seeded/nylon substrate are investigated.
3. Highly flexible MSM UV-PDs and H_2 gas sensor devices are fabricated.
4. DHS-MCBD as a novel technique for forming ultra-long ZnO NRs arrays on Si seeded and GaN seedless substrates is used.

5. DHS-MCBD technique is used to fabricate a nano-size junction between ZnO NRs and p-GaN layer, and as a result, a high-extraction-intensity light emitting diode (LED) was successfully fabricated.
6. The present work provides the ultaralong and ultradensity of ZnO NRs on the seeded and seedless substrates, and fabrication of a nanojunction device such as LED. What differentiates this work from the previous ones is that a substrate is directly heated (DHS) meanwhile the precursor solution is not exposed to the heat by any external heat sources. After an extensive literature review, it was concluded that no study has been reported on synthesis of ultralong ZnO NRs and the fabrication of LED device based on nanosize junction by modifying CBD method.

1.4 Thesis Overview

This thesis consists of eight chapters and organized as follows: **Chapter 1** a brief introduction of ZnO material, its synthesis methods, and its applications. The problem statements are presents. Objectives of the project, and thesis originality are presented. **Chapter 2** presents a literature review on general properties of ZnO material and ZnO NRs prepared by hydrothermal and DH-MCBD techniques. Flexible MSM UV-PD, flexible H_2 gas sensing, and LED devices are also included. Sensing mechanism of UV photodetector and H_2 gas sensor are discussed. The working principles of LED with radiative recombination mechanisms are also discussed. **Chapter 3** describes the methodology and instrumentation used to analyze the prepared material and fabricated MSM UV-PDs, H_2 gas sensor, and LED devices. The results obtained are characterized and discussed in the next chapters. **Chapter 4** presents the characterization results and discussion of the fabricated

MSM UV-PDs, which is highly flexible. The effect of heat treatment duration applied to the ZnO seeded/nylon substrate is also studied. **Chapter 5** presents the characterization results and discussion of the highly flexible MSM H_2 gas sensor, that was fabricated. **In Chapter 6** morphological, structural, and optical properties of the as-grown ultralong ZnO NRs on silicon and p-GaN substrates are investigated, and then the fabrication and characterization of a nano-size junction LED are discussed. Finally, the conclusions of this study with possible future researches are presented **in Chapter 7**.

CHAPTER 2: LITERATURE REVIEW AND THEORETICAL BACKROUND

2.1 Introduction

In this chapter, general properties of ZnO material, its synthesis methods as nanorods, and some of its applications such as MSM-photodetector, gas sensor, and LED devices are presented. Two methods are discussed; hydrothermal growth ZnO NRs on a novel highly flexible nylon substrate and DHS-MCBD as a novel technique for the growth of ultralong ZnO NRs on seeded and seedless substrates. Finally, a summary, review of articles, and theoretical background concerning the use of ZnO NRs in ultraviolet (UV) detection, H_2 gas sensing, and light-emitting diode (LED) are discussed.

2.2 General Properties of ZnO

ZnO is a II-VI group compound semiconductor material having a hexagonal (wurtzite-type) structure with lattice parameters at room temperature a = b = 0.3245 nm and c= 0.52066 nm [27]. Additionally, other favorable aspects of ZnO material are that it is cheap, non-toxic, relatively abundant source materials, and chemically stable [28]. The as-grown ZnO material, especially in case of the low growth temperature, is unintentionally n-type, and it is typically believed that it possesses many native defects, such as oxygen vacancy (V_o), interstitial zinc (Z_{ni}), zinc vacancy (V_{zn}), interstitial oxygen (O_i), and background impurities such as hydrogen are source of donors in ZnO. These defects are responsible for the deep level emissions (DLEs) [29, 30].

2.2.1 Crystal Structure Properties of ZnO

In fact, ZnO crystallizes stably at normal atmospheric pressure and thermodynamically in the hexagonal wurtzite structure, but it can be also in the zinc-blende structure, which can be stable when ZnO growth started from surface of the cubic substrates structure, such as ZnS. Figure 2.1 shows crystal structure model of hexagonal wurtzite ZnO, the clarification of its wurtzite structure is not complex. The wurtzite ZnO structure consists of alternating zinc (Zn) and oxygen (O) atoms, where each oxygen ion (O^{2-}) is surrounded tetrahedrally by four zinc ions (Zn^{2+}), and vice versa. The ZnO structure has two polar surfaces the polar Zn (0001) and O (0001) terminated faces, and has other two most commonly of non-polar (1120) and (1010) surfaces possessing an equal number of Zn and O atoms [31, 32].

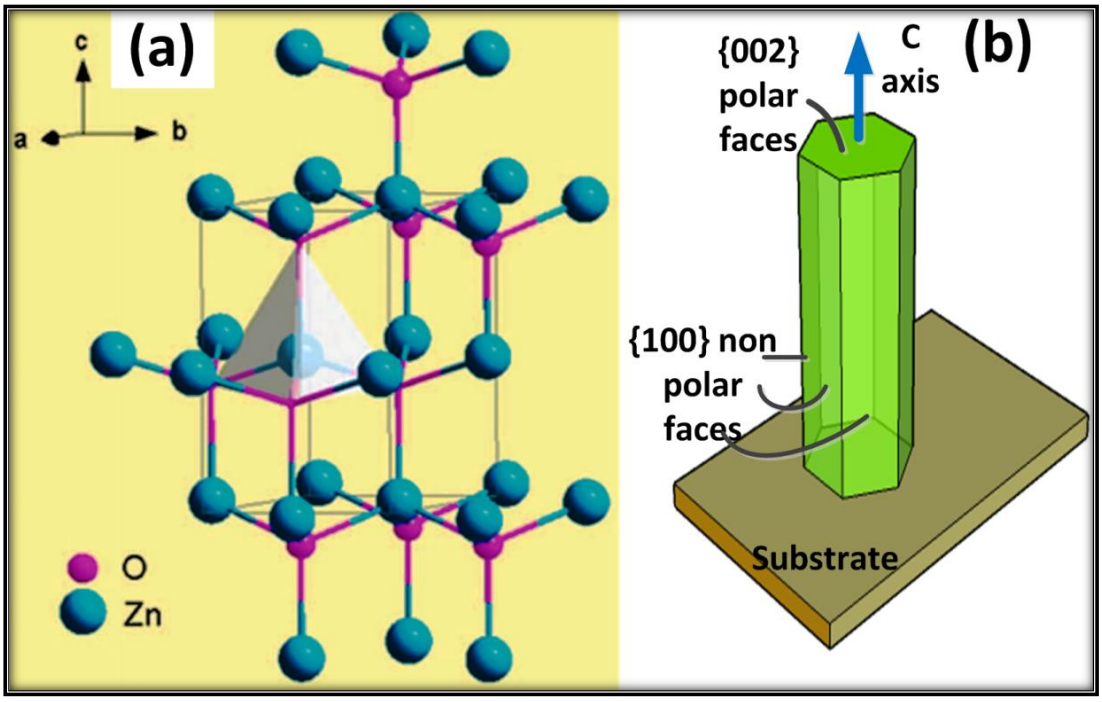

Figure 2.1: Crystal structure model of hexagonal wurtzite ZnO (a) hexagonal wurtzite crystal structure of ZnO [31], (b) polar faces, perpendicular to the [0001] direction, and non-polar faces, parallel to the [0001] direction [32].

The polar surfaces are very important characteristic of ZnO. It has a normal dipole moment along the c-axis due to the oppositely charged ions for Zn^{-} and O^{-}, and that lead to the production of positively charged (0001) and negatively charged $(000\bar{1})$ surfaces, respectively. Also, ±(0001) surfaces of ZnO are atomically stable, flat and without surface reconstruction, therefore it can be considered that the structure of ZnO is somewhat stable [33].

2.2.2 Optical Properties of ZnO

ZnO semiconductor is of great interest because of its significant and unique properties, such as: large direct band of 3.37 eV, large exciton binding energy of 60 meV at RT, and high light trapping characteristics [27, 34]. Therefore, ZnO semiconductor is among the most promising and beneficial materials for an enormous range of nanotechnology applications, such as ultraviolet (UV) detectors, chemical sensors, biosensors, pH sensors, and UV blue light emitting devices [3]. Generally, direct band gap materials have essentially high luminescence yield compared to indirect band gap materials, and large band gap materials are useful for reducing the leakage current of the devices.

Higher exciton binding energy materials give brighter emissions, because exciton is already a bound system, which radiatively recombine with high efficiency without requiring traps to localize the carriers [35]. Optical properties of crystalline ZnO were mostly studied by the absorption or photoluminescence (PL) spectra. The absorption spectrum of the ZnO shows high transparency in the visible region and at long wavelengths ($\lambda > 380$ nm) as well as strong UV absorption at short wavelengths ($\lambda < 380$ nm), while ultraviolet (UV) emission peak and visible emissions are commonly observed in PL spectrum. Generally, UV emission peak of ZnO, which

represents the near-band-edge emission (NBE) of the wide ZnO band gap, is located at approximately 378 nm (3.28 eV), which resulted from the recombination of the free exciton process.

The PL spectra also reveals broad visible peaks that were related to the deep level emission (DLE) of ZnO, which was attributed to the native defects in ZnO NRs. In fact, the broad visible peaks are observed in the wavelength range starting approximately from 400 nm to 720 nm. However, the origins of deep level emissions of ZnO are still not fully understood, and many researchers suggested different and controversial explanations for these defect emissions (violet, blue, green, orange-red, and red). For example, many researchers have suggested that, within the DLE, the green emission has originated from both oxygen and zinc vacancies [36, 37], while other authors have reported that the green emissions can be attributed to oxygen vacancies (V_o) and zinc interstitial (Zn_i) [38, 39].

In fact, the origins of the ZnO PL emissions, especially for ZnO defect energy levels, are a complicated process and still not completely understood. However, theoretically, the positions of the Z_{ni}, zinc vacancy (V_{Zn}), V_o, and oxygen interstitials (O_i) are located at 0.22 eV, 3.06 eV, 2.47 eV, and 2.28 eV below the conduction band, respectively [40]. Figure 2.2 illustrates the schematic band diagram of the DLE emissions in ZnO, which presents the recombination of electron-hole pairs from different defects back to the valence band and which lead to emission of photon energy [41, 42]. The value of I_{UV}/I_{DLE} ratio (the intensity of the UV emission to the visible deep level) play important role to determine the quality and amount of defects in the ZnO material, in which this high difference in intensity suggests that the grown

ZnO NRs arrays have high quality with small number of defects, and a good hexagonal structure [43, 44].

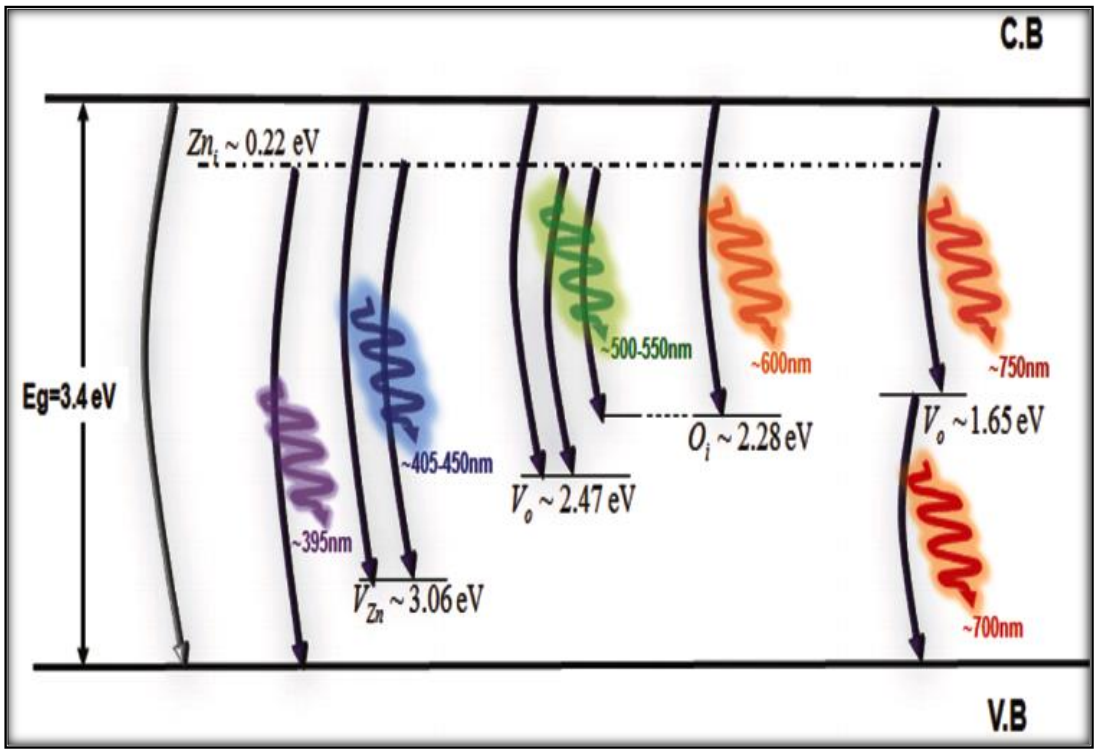

Figure 2.2: Schematic energy level diagram of various defect level emissions in ZnO [41, 42].

2.3 Growth Methods of ZnO NRs

Several synthesis methods have recently been developed for 1D ZnO nanomaterial growth, including metal–organic chemical vapor deposition (MOCVD) [6, 7], hydrothermal or wet chemical methods [4], physical vapor deposition (PVD) [12, 13], molecular beam epitaxy (MBE) [5], pulsed laser deposition (PLD) [8], sputtering [14], top-down approaches by etching [9], eletrospinning [10, 11] and so on. In this context, it is essential to show the difference between three important terms, hydrothermal, solvothermal, and CBD. Hydrothermal process includes the use of supersaturated aqueous (water) as the solvent of the material used inside a closed

vessel under high temperature and pressure in order to prepare and crystallize the nanomaterials.

Solvothermal method includes an organic solvent used instead of water inside a closed vessel under high temperature and pressure. As for CBD method, similar to hydrothermal method, water is used as the solvent of the other materials, but under low temperature (less than 100 °C) and the reactions is inside an opened vessel (under ambient pressure) [45, 46]. However, the system used for the fabrication of nanomaterials in both methods, hydrothermal and CBD, is the same but the vessel that contains the solution in the first method, hydrothermal, should be tightly closed, while in the second method, CBD, is not necessary to be closed.

2.3.1 Growth Mechanism of ZnO NRs by CBD Method

In CBD method (or hydrothermal method), in order to grow the units of ZnO NRs two ions are needed, namely, Zn^{2+} and OH^-. These ions have a significant function in producing colloidal $Zn(OH)_2$ clusters. In all experiments in this project were used the most common chemicals, zinc nitrate hexahydrate $Zn(NO_3)_2$. $6H_2O$ and hexamethylamine (HMTA) $C_6H_{12}N_4$. Zinc nitrate salt provides Zn^{2+} ions required for building up the ZnO NRs, while water molecules in the solution provide O^{2-} ions. Even though the exact function of HMTA during the ZnO NRs growth is still under investigation, it is believed to serve as a weak base and slowly hydrolyzing in the water solution to supply OH^- ions [47, 48].

The chemical reactions for the growing of ZnO NRs can be summarized into the following four steps: decomposition reaction Eq. (2.1), hydroxyl supply reaction Eq. (2.2), supersaturation reaction (Eq. (2.3) and Eq. (2.4), and ZnO nanowire growth reaction Eq. (2.5) [35, 49, 50]:

$$C_6H_{12}N_4 + 6H_2O \rightarrow 6HCHO + 4NH_3 \quad (2.1)$$

$$NH_3 + H_2O \rightarrow NH_4^+ + OH^- \quad (2.2)$$

$$Zn(NO_3)_2 \rightarrow Zn^{2+} + 2NO_3^- \quad (2.3)$$

$$Zn^{2+} + 2OH^- \rightarrow Zn(OH)_2 \quad (2.4)$$

$$Zn(OH)_2 \rightarrow ZnO + H_2O \quad (2.5)$$

Four main parameters, namely, precursor materials, precursor concentration, duration and temperature have significant influence in controlling structure stability, morphology and optical properties of nanomaterials produced by CBD method. In this context, the polar surface of ZnO has higher energy, therefore it plays an important key role in the column growth. The polar {001} surfaces have approximately 60% higher cleavage energy than the nonpolar {100} and {110} faces [51]. Therefore, due to this difference in the surface energy of different crystal planes, the high-energy surface, {001}, would grow faster than other lower energy surface. Therefore, in the case of the formation of 1D ZnO nanostructures, this process is repeated during ZnO crystallization, thus leading to a growth rate along the $[001]$ direction to be faster than other directions (Figure 2.1 (b)) [45, 52, 53].

It is worth mentioning that the ZnO seed layer play an important role for the growth of well aligned ZnO NRs arrays on the substrate by CBD method. the presence of the ZnO seed layer on the substrate lead to decreasing significantly in the interface energy between ZnO crystal and the substrate, as a consequence, the nucleation process occur quickly and the NRs -arrays can grow more easily [54, 55].

2.3.2 Hydrothermal Growth of ZnO NRs on Highly Flexible Nylon

In general, ZnO materials can be grown experimentally on rigid or flexible substrate. However, flexible substrates offer several advantages and valuable properties compared with rigid substrates, including transparency, transportability, flexibility, small volume, light weight, high resistance to damage, and low cost. Several types of polymer substrates can be used as flexible substrates, such as flexible Kapton, polyimide, polyethylene terephthalae, polyethersulfone, and polyethylene naphthalate [56, 57]. A flexible transparent substrate has an amorphous structure.

Hydrothermal method is usually adopted to synthesize ZnO NRs. The method offers some advantages such as low deposition temperature and does not require any harsh fabrication process of target substrates. This enables the use of unconventional substrates such as a plastic, polymer, fabric, and paper due to flexible polymer substrates also have a low heat resistance at high-temperature processes. However, because of the low temperature, this method faces some disadvantages, such as poor crystallinity and high defects concentration, which weakens the device's performance (especially when compared with other high temperature methods such as chemical vapor deposition (CVD) [58]. In many works reported so far, the authors have used thin flexible substrates such as a flexible Kapton (50 μm) as substrate to grow vertically ZnO NRs [56, 57], for developing UV detector and H_2 gas sensor [59].

2.3.3 Direct Heat Substrate-Modified Chemical Bath Deposition (DHS-MCBD) Technique for Growth of Ultralong ZnO NRs

Both synthesis methods, hydrothermal and CBD have many advantages to synthesis of ZnO NRs and both have attracted great interest by researchers. The

fabrication of ultralong ZnO NRs by these methods is still challenging, all the reasons anticipated for this problematic issue were mentioned and have been explained in section 1.1. To address these problems, researchers have used many strategies in order to increase the length of ZnO NRs arrays for high aspect ratio of ZnO NRs where this could lead to increase in efficiency for the devices fabricated.

However, there were several reports on hydrothermal synthesis of ultralong ZnO NRs by using different precursor materials as ions source, instead of the aqueous zinc nitrate- hexamethylamine HMTA. Hua *et al*. reported the synthesis of ZnO NRs with large aspect ratio by using zinc nitrate hexahydrate and HMTA with aluminum iso-propylate. They prepared ZnO NRs arrays with a length of 10 μm and aspect ratio of 70. Nevertheless, the significant improvement in the aspect ratio requires far more effort by this method, due to that their method was based on the principle of addition of aluminum-iso-propylate and the number of cycles for the enhancement of the aspect ratio [60].

There are also other precursors which have been used by the researchers for ultralong growth of nanorods. Xu *et al*. reported the growth of ultralong ZnO NRs (length up to 30 μm within 10 h) using zinc hydroxide, ammonium hydroxide, polyethyleneimine (PEI), and seed nanoparticles [61]. Qiu *et al*. used the PEI-assisted preheating hydrothermal method (PAPHT) to prepare ZnO NRs arrays with a long length of more than 40 μm [62]. Recently the continuous flow injection (CFI) hydrothermal synthesis reaction was used by several researchers to obtain ultralong ZnO NRs arrays. For instance, Chen *et al*. have shown that a continuous flow of Zn precursors can yield ultralong ZnO nanowires by hydrothermal method. Zinc acetate dihydrate and HMTA were continually injected to the complex reactor for ZnO

growth. The concentration of the reactor was refreshed every 4 h and a 24 h of growth yield a length of 15 μm [63].

To obtain an ultralong ZnO nanorod on a substrate by the CBD or hydrothermal methods, the growth of ZnO rod should be accelerated. Due to the length of the ZnO NRs increased with increasing the temperature [64], therefore, It is believed that the best way to accelerate the growth of ZnO rods can be by increasing the temperature of a substrate, in other words, by increasing the supply of energy on a substrate. Temperature here can be referred as solution temperature or substrate temperature. The vast majority of the researchers have focused in their research on the effect of a solution temperature and not a substrate temperature on growth of ZnO NRs or other materials via hydrothermal method.

However, there is maybe one report, somewhat similar to this work with some important differences. Tae Lee and his group constructed a system for a modified CBD method by heating a seeded substrate directly on a hot plate which continuously delivers a constant concentration of hot solution (80 $^{\circ}$C) to the seeded substrate. [65]. However, this group did not mention about nanosize-junction because of they used only ZnO seeded silicon as the substrate, and they did not fabricate any kind of nanosize electrical device. In this context, the fabrication of nanorods of high aspect ratio with length typically more than 100 μm are still difficult and challenging by a low temperature method. However, a high temperature method provides an easy way to obtain high length of ZnO NRs. It is worth mentioning that the main advantage of the high temperature technique is the growth of high quality single crystalline nanowires which are mandatory for electronic and optoelectronic

applications. Table 2.1 summarizes the results reported by several groups on the growth of ultralong ZnO NRs.

Table 2.1: The diameter, length and aspect ratio of ZnO NRs grown using different fabrication methods and reported by several groups.

Synthesis method	Growth temperature (°C)	Growth time	Diameter (nm)	Length (µm)	Aspect ratio	Ref.
Hydrothermal	75	28 h	~140	~10	~70	[60]
Hydrothermal	88	10 h	150-300	~30	~133	[61]
Hydrothermal	85	24 h	~120	~15	~125	[63]
Anodization	70	4 h	~100	~100	~1000	[66]
Carbothermal	917	15 min	100-300	~100	~500	[67]
Vapour Phase Transport	950	40 min	100-200	~180	~1200	[68]

2.4 Metal-Semiconductor-Metal (MSM) Photodetector

Metal–semiconductor–metal photodetector (MSM-PD) was first proposed and demonstrated by Sugeta *et al.* in 1979 [69]. Since then, many research groups started to improve and develop the fast response, high sensitivity and high speed MSM-PDs [70]. Fundamentally, a conventional MSM-PD is a symmetrical device matching to two Schottky connected back-to-back diodes on a semiconductor layer. When a voltage is applied, one of the contacts (electrodes) of interdigitated fingers is foreward-biased and the other one is reverse-biased, and so on [71]. The conventional MSM-PD structure is shown in Figure 2.3 (a). When the conventional device is illuminated by light from the top on surface, a significant amount of this incident light is reflected, especially from the top surface of the fingers, which was

fabricated from a metal. Therefore, only the area of the exposed surface for the semiconductor layer of the device will interact with the incident light.

In fact, the active area of light absorption is the area of semiconductor between the metal fingers. When the light which has energy greater than the bandgap energy of the semiconductor is incident on the top of the MSM device surface, electron–hole (e–h) pairs are generated, as shown from cross-sectional views of device in Figure 2.3 (b). The carriers are transferred to the metal contact pads without or with applied external bias voltage and current are detected in the external circuit under the application of an external bias voltage. MSM-PDs are extremely important in optical communication systems and other applications because they present a variety of benefits such as simplicity of fabrication, high-current gain, small dark current, high responsivity and high-speed operation.

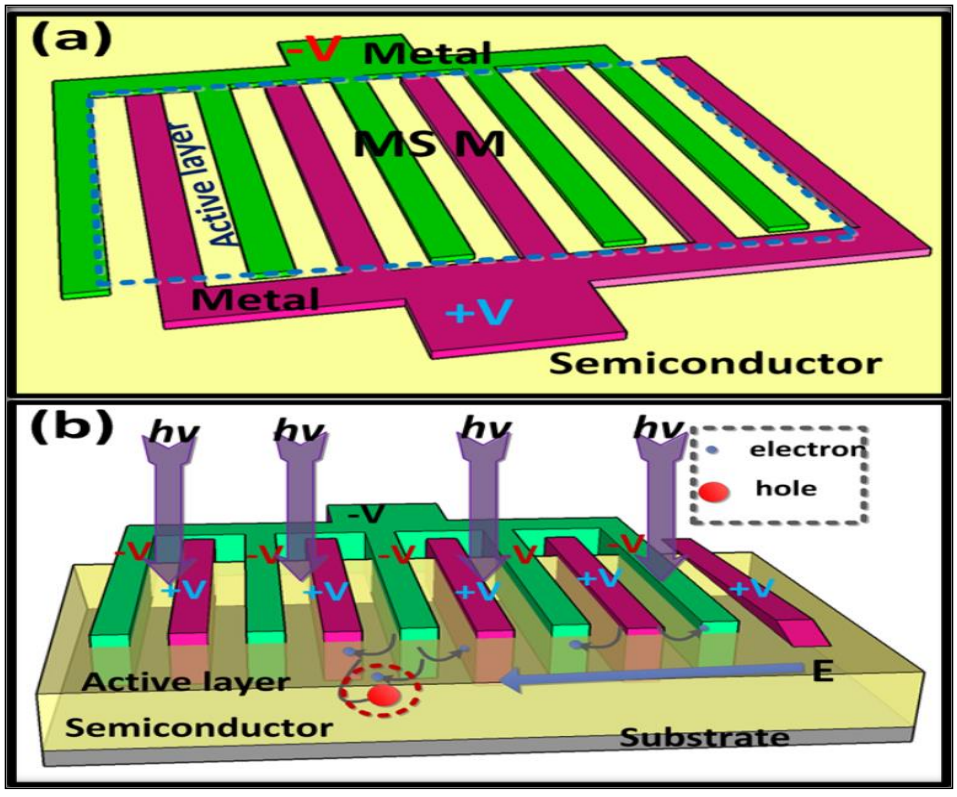

Figure 2.3: A structure of a conventional MSM-PD: (a) the top of the surface and (b) cross-sectional views.

2.5 Operational Parameters of Photodetectors

There are some important parameters of MSM-PD which are of interest such as, current gain and responsivity.

2.5.1 Current Gain

The current gain is an important parameter, which is useful to evaluate photo-detection ability. It represents the ratio of photocurrent to dark current, which can be calculated by the following equation:

$$\text{Current gain} = \frac{I_{ph}}{I_d} \tag{2.6}$$

where I_{ph} is the photocurrent generated, when the device is under incident light and I_d, is the dark (leakage) current which was generated with no incident light [72]. It is worth to mention that to enhance current gain for MSM-PD, the leakage current should be decreased and the photocurrent increased for the device.

2.5.2 Responsivity

The responsivity (R) of as-fabricated MSM-PD device is defined as the ratio of the electrical output to the optical input for a given wavelength and can be calculated using the following equation [73]:

$$R = \frac{I_{ph} - I_d}{P_{op}} = \frac{I_{ph} - I_d}{E_{op} \cdot A} \tag{2.7}$$

where I_{Ph} is the photocurrent which was generated per unit optical power of incident light (P_{op}) on the effective area of the device (A), I_d is the dark current, and E_{op} is the irradiance of light. According to some previous reports, a high surface-to-